RTk/S$_N$ SOLUTIONS OF THE 2D MULTIGROUP TRANSPORT EQUATIONS IN HEXAGONAL GEOMETRY

E. del Valle
Escuela Superior de Física y Matemáticas
Instituto Politécnico Nacional
07738 México D.F. (Mexico)
edmundo@esfm.ipn.mx

and

Ernest H. Mund
Service de Métrologie Nucléaire (CP 165/84)
Université Libre de Bruxelles
B-1050 Brussels (Belgium)
emund@ulb.ac.be

ABSTRACT

We present an extension to the hexagonal geometry of some weakly discontinuous nodal finite element schemes developed by Hennart and del Valle for the two-dimensional discrete ordinates transport equation in quadrangular geometry. This extension is carried in a similar way as the extension to the hexagonal geometry of nodal element schemes for the diffusion equation using a composite mapping technique suggested by Hennart, Mund and del Valle. The combination of the two techniques (i.e. the weakly discontinuous scheme and the composite mapping) is new. It is detailed in the main section of the paper. The algorithm efficiency is shown numerically through some benchmark calculations on classical problems widely referred in the literature.

1. INTRODUCTION

Nodal finite element methods in quadrangular geometry are very flexible solution techniques for diffusion and transport problems (see [1-3]). They provide analytical expressions of the solution in the whole domain. Furthermore, they easily allow both mesh refinement and increase of polynomial degree (the so-called *hp* approach of the finite element technique [4]) to enhance the numerical accuracy of the solution. With regard to multidimensional diffusion equations, the main theoretical results can be found in [5]. With regard to the transport equation, Hennart and del Valle have shown that, for one-dimensional problems, the family of discontinuous moment methods developed in [3] converge to the exact solution of the transport equation with increasing polynomial degree. No such result has yet been proven for multidimensional problems, but numerical results suggest that it is likely to exist.

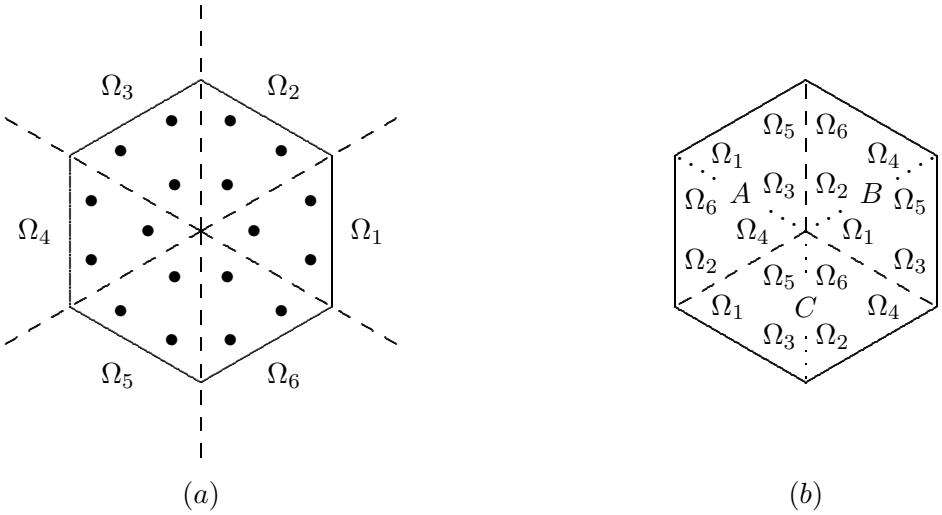

Figure 1: The DIAMANT2 angular sectors and discrete ordinate data set for the S_4 approximation (a). The angular sectors in the losange partitioning of a generic hexagon (b).

Clearly, one would also like to have efficient algorithms for the transport equation in the hexagonal and hexagonal-z geometries. Hexagonal geometry is more difficult to handle though, except if one looks at a single hexagon as a composite domain made of three or four trapezoidal subdomains, easily mapped onto the 2D reference domain $\overline{V} \equiv [-1,+1] \times [-1,+1]$. This idea has already been used independently by Azmy (see [6]), and by Hennart, Mund and del Valle (see [7]) to solve the multigroup diffusion equations in hexagon arrays. While, the latter authors built their algorithm on a hexagon partition into four trapezoids and a subsequent iterative preconditioning solution technique based on nodal finite elements, Azmy used a hexagon partition into three losanges in a nodal integral framework. The present study also uses a losange partitioning of the hexagons. Section 2 of the paper describes the basic formalism combining a mapping of the losanges onto $\overline{\Omega}$ and the weakly discontinuous (WD) algorithm proposed by Hennart and del Valle, for the solution of the multidimensional transport equation in quadrangular geometry [8]. Only a subset of the WD algorithms having robust convergence properties (in 1D transport cases), the Raviart-Thomas schemes RTk is used in this work. This section also gives some details about the implementation of the algorithm. Section 3 discusses the numerical results, when the algorithm is applied to classical benchmark problems. Finally, Section 4 draws the conclusion.

2. BASIC FORMALISM

For the sake of simplicity we consider the one group transport equation in 2D, in a physical domain V, union of hexagonal reactor assemblies with homogeneous neutron properties :

$$\mu_k \frac{\partial \psi_k}{\partial x} + \nu_k \frac{\partial \psi_k}{\partial y} + \Sigma_t \psi_k \; = \; Q_k, \qquad (x,y) \in V, \qquad k = 1, \ldots, M. \tag{1}$$

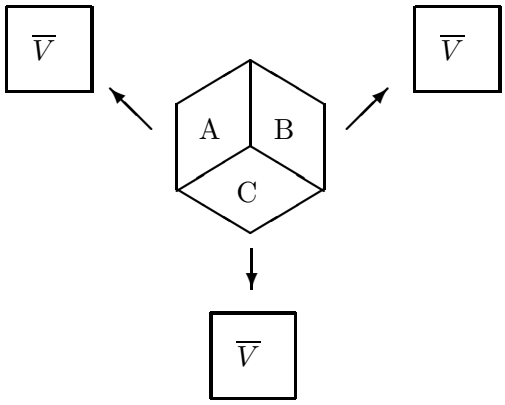

Figure 2: A hexagon decomposition and the reference domain $\overline{V} = [-1, +1]^2$.

In this equation ψ_k denotes the angular flux corresponding to the k-th ray of the S_N approximation with angular coefficients μ_k and ν_k, M being the total number of rays. The right-hand side Q_k denotes some neutron source that may include for instance scattering and fission. Henceforth we adopt the set of discrete ordinates (DOs) used in the DIAMANT2 code that are tailored to the triangular geometry (see [9]). Accordingly, the unit sphere is divided into twelve "dodecants" and the total number of rays associated to the S_N approximation is $M = 3N(N+2)/4$. Since the present work is done in 2D, the dodecants reduce to sextants $(\Omega_1, \ldots \Omega_6)$ displayed on Fig. 1.a. The dots denote the DOs corresponding to the S_4 approximation. The right part Fig. 1.b shows the distribution of the angular sectors (i.e. the sextants) in the hexagon.

2.1 THE HEXAGON PARTITIONING TECHNIQUE

In our numerical scheme, a generic hexagon is decomposed into three losanges as shown on Fig. 2. Using the Gordon blending technique outlined in [7], each losange may be mapped onto the reference interval $\overline{V}$, as suggested on the figure. Considering losange A, for instance, the relationship between the physical coordinates (x, y) and the transformed coordinates (ξ, η) in $\overline{V}$, writes:

$$\begin{aligned} x &= a(\xi - 1)/2, \\ y &= b(\eta + (\xi + 1)/2), \end{aligned} \tag{2}$$

where the constants a and b are related to the size of the hexagon. Denoting by R the length of a hexagon side, it is easy to show that $a = R\sqrt{3}/2$ and $b = R/2$. Analog expressions to (2) may be derived for the losanges B and C.

After mapping the three subdomains onto $\overline{V}$, the transport equation (1) becomes

$$\mu'_k \frac{\partial \psi_k}{\partial \xi} + \nu'_k \frac{\partial \psi_k}{\partial \eta} + \overline{\Sigma}_t \psi_k \;=\; \overline{Q}_k, \qquad (\xi, \eta) \in \overline{V}, \qquad k = 1, \ldots, M, \tag{3}$$

where the directions (μ'_k, ν'_k) depend on the losange being mapped. The quantities $\overline{\Sigma}_t$ and $\overline{Q}_k$ denote "scaled" cross sections and source terms. Considering again losange A, one gets

$$\mu'_k = \mu_k, \qquad \nu'_k = \left(\frac{\nu_k \sqrt{3} - \mu_k}{2} \right), \tag{4}$$

and

$$\overline{\Sigma}_t = \frac{\sqrt{3}R}{4}\Sigma_t, \qquad \overline{Q}_k = \frac{\sqrt{3}R}{4}Q_k. \tag{5}$$

Similar expressions may be obtained for the losanges B and C. One verifies easily that angular directions corresponding to acute angles are stretched while those corresponding to obtuse angles are compressed. It should be emphasized also that stretched and compressed angular directions in the three losanges are not the same so that different (but equivalent) data sets for a given discrete ordinate method must be adopted in each losange.

2.2 THE WEAKLY DISCONTINUOUS SCHEME

Each equation (3) is then solved using the RTk nodal scheme, a subclass of the WD schemes described in [8], on a partition of $\overline{V}$ with $I \times J$ nodal elements, taking into account the neighboring cells. Since this scheme is central to our algorithm, we recall its basic definition. For the sake of convenience, we use henceforth the Cartesian coordinates (x, y) instead of (ξ, η).

Assume $\overline{V}$ has been discretized into $N_e := I \times J$ cells V_e, (i.e $\overline{V} = \cup_{e=1}^{N_e} V_e$) where each cell itself, as is traditional with the finite element method, is mapped onto the reference cell $\overline{V}$. A particular nodal element is defined by a set of degrees of freedom D and a space of (polynomial) functions S with $card(D) = dim(S)$. The degrees of freedom are either cell and/or edge moments, hence the name of *nodal* finite elements.

To describe D and S in a compact way, we introduce some convenient notation. Let P_i be the normalized Legendre polynomial of degree i over $[-1, +1]$ which satisfies the relationships :

$$P_i(+1) \,=\, 1, \quad P_i(-1) \,=\, (-1)^i, \quad \text{and} \quad \int_{-1}^{+1} P_i(x)\, P_j(x)\, dx \,=\, N_i \delta_{ij}, \tag{6}$$

with $N_i = 2/(2i + 1)$. In addition, we define $P_{ij}(x, y)$ as $P_i(x)P_j(y)$. Assuming that $L\psi = Q$ is the equation to solve, $\psi(x, y)$ is approximated by $\psi_h(x, y) \in S$ and over $\overline{V}$ cell moments of ψ_h are defined by :

$$\psi_C^{ij} := \int_{-1}^{+1} \int_{-1}^{+1} P_{ij}(x, y)\psi_h(x, y)\, dxdy/(N_i \cdot N_j). \tag{7}$$

Similarly, edge moments are defined by :

$$\psi_E^i := \int_{-1}^{+1} P_i(s_E)\psi_h(x_E, y_E)\, ds_E/N_i, \tag{8}$$

where E is a generic symbol corresponding to L, R, B or T, for the left, right, bottom, or top edges respectively, x_E or y_E being equal to ± 1 depending on the particular edge considered, the other coordinate being s_E, the coordinate along that edge.

To define the space of functions S, we introduce the spaces of polynomials of degree i in x and j in y, $\mathcal{Q}_{ij}(x, y) \equiv \{x^a y^b \,|\, 0 \le a \le i, 0 \le b \le j\}$, with in particular $\mathcal{Q}_i \equiv \mathcal{Q}_{ii}(x, y)$, and also the spaces of polynomials of degree i in x and y, $\mathcal{P}_i(x, y) \equiv \{x^a y^b \,|\, 0 \le a + b \le i\}$, where a and b are integers. With these definitions in mind, the RTk nodal finite elements where k is an arbitrary nonnegative integer may be characterized as follows :

$$RTk \quad = \quad [D \equiv \{\psi_E^i, \psi_C^{ij},\ i, j = 0, \ldots, k\},\ S \equiv \{\mathcal{Q}_{k+2\,k}(x, y) + \mathcal{Q}_{k\,k+2}(x, y)\}]. \tag{9}$$

The element has $N_p(k) = (k + 1)(k + 5)$ degrees of freedom. On each cell V_e, the angular flux is approximated by :

$$\psi_h(x, y) \,=\, \sum_E \sum_{i=0}^{k} \psi_E^i\, u_E^i(x, y) \,+\, \sum_{i,j=0}^{k} \psi_C^{ij} u_C^{ij}(x, y), \tag{10}$$

where the basis functions u_E^i and u_C^{ij} have very compact expressions in terms of the Legendre polynomials $P_{ij}(x, y)$. For more detail the reader is referred to [1].

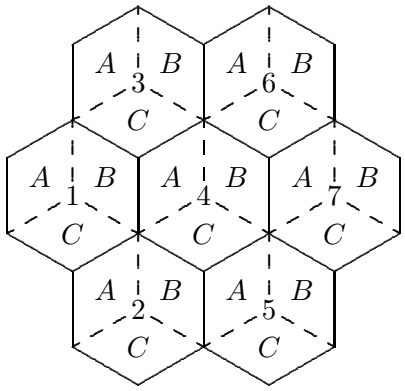

Figure 3: A set of hexagons illustrating the solution strategy

Replacing ψ by ψ_h in each cell V_e, a local residual $L\psi_h - Q$ arises. If the ray (μ', ν') is in the *first* quadrant, one proceeds cell by cell by a standard diagonal sweep beginning with the first cell seen by the particular ray considered. Consequently, one knows from the boundary conditions at the left or bottom of the domain (or from the left or bottom neighbors which have been processed previously) the edge moments on the left and bottom edges if, as is the case with the WD methods, some of these moments are conserved between neighbors.

Locally, cell Legendre moments of the residual $L\psi_h - Q$ are taken to obtain as many equations as unknowns. Since L is a *first order* differential equation, its application to a discontinuous approximation generates delta distributions and the correct way to take these distributions into account is to derive the moment equations over a cell V_e which is shifted upstream by ϵ, in the limit of vanishing ϵ.

For a ray in the first quadrant, that means that the cell considered is moved slightly downward and to the left. As $\epsilon \to 0$, boundary terms arise at the left and at the bottom of the cell, connecting it to its upstream neighbors or boundaries. This *upwinding* procedure is classical when discontinuous approximations are used for first-order equations. After taking the ϵ-limit, the (ij) cell moment equation reads :

$$\begin{aligned} & \int_{y_B}^{y_T} \{\mu' p_{ij}(x_L, y)[\psi_h(x_L + 0, y) \, - \, \psi_h(x_L - 0, y)]\} \, dy \\ + & \int_{x_L}^{x_R} \{\nu' p_{ij}(x, y_B)[\psi_h(x, y_B + 0) \, - \, \psi_h(x, y_B - 0)]\} \, dx \\ + & \int_{V_e} p_{ij}(x, y)(L\psi_h(x, y) \, - \, Q) \, dxdy = 0, \end{aligned} \tag{11}$$

where $p_{ij}(x, y)$ denotes the Legendre polynomials P_{ij} scaled to the cell $V_e \equiv (x_L, x_R) \times (y_B, y_T) \subset (-1, +1)^2$.

For the WD schemes, the first two terms in Eq. (11) vanish by definition. Let N_u denote the number of unknowns per cell. For the weakly discontinuous RTk case with $2(k + 1)$ edge moments conserved from cell to cell, $N_u(k) = (k+1)(k+3)$. Selecting N_u basis functions among the elements of S, Eq. (11) gives a set of equations for the unknowns. For a ray in the first quadrant, these unknowns are the cell moments and the edge moments on the top and right edges. The procedure must be carried for all quadrants. Moments conservation changes from

quadrant to quadrant. Finally, we mention that the WD Raviart-Thomas algorithms correspond to the $WD_{N_p(k)\,N_u(k)}$ schemes described in the reference [8].

2.3 ALGORITHM IMPLEMENTATION TECHNIQUE

An essential feature of the algorithm is the selection of a strategy to sweep the losanges in the reactor domain V and the ordering of the unknowns. With regard to the latter, we have again adopted the convention used in the DIAMANT2 transport code [7]. The strategy to sweep the losanges in the reactor domain however, is specific to this study and perhaps not optimal. It is best explained with the example displayed on Fig. 3 of a central hexagon surrounded with a ring of 6 hexagons. All hexagons have been numbered from 1 to 7 and partitioned into the losanges A, B and C as shown on the figure. For a single hexagon the computation of the angular fluxes

Table 1: Losange (a) and hexagon (b) ordering for the sweep of the discrete ordinates $\vec{\Omega}$ belonging to Ω_k, $(k = 1, \ldots, 6)$ in the example displayed on Fig. 3.

	Ω_1	Ω_2	Ω_3	Ω_4	Ω_5	Ω_6
a	ACB	CAB	CBA	BCA	BAC	ABC
b	1 2 3 4 5 6 7	2 1 5 4 3 7 6	5 7 2 4 6 1 3	7 6 5 4 3 2 1	6 3 7 4 1 5 2	3 6 1 4 7 2 5

may be done by solving the discretized neutron transport equations for all discrete ordinates belonging to a given sextant Ω_k, $(k = 1, \ldots, 6)$ where the basic losanges are swept in the order given in (a, Ω_k) in Table 1. However, for the array displayed on Fig. 3, the numerical scheme governing the sweep of the hexagons is more complicated for topological reasons. In algorithmic form, it runs as follows :

For $k = 1, \ldots, 6$,
  For all hexagon assemblies in the order set in (b, Ω_k),
    For all DOs $\vec{\Omega} \in \Omega_k$,
      Compute the angular flux in the losanges in the order set in (a, Ω_k).
    EndDo
  EndDo
EndDo

At the end of the procedure each losange in the V domain must have been swept once for each angular direction in the S_N approximation. A generalization of the procedure can easily be built to solve transport problems in more complicated hexagonal arrays.

As a last comment on our hexagonal nodal transport scheme, we emphasize that the set of multigroup transport equations is solved using the conventional fission source iteration technique with LU factorization for the individual group problems. For practical reasons we restrict the present numerical assessment of the RTk schemes to $k = 0, 1$. Higher values of k, though straightforward to implement, lead to more time consuming calculations and will be studied later on.

3. NUMERICAL RESULTS

The methodology described in this paper has been implemented into a computer code named **THG** (for **T**ransport in **H**exagonal **G**eometry). To assess the numerical efficiency of the code,

we have run several multigroup benchmark problems with decreasing mesh sizes or/and increasing polynomial degrees. All the computations were carried on an Alpha workstation in single precision with the S_4 angular approximation. The benchmark problems were the following: 1/ a simplified hexagonal core proposed in Ref. [11] (see Fig. 4 and Table 2), 2/ a modified SNR benchmark problem also proposed in [11,12] (see Fig. 5 and Table 3), and 3/ the 2D-KNK benchmark problem [12] (see Fig. 6 and Table 4) referred as "Model 4" in [10].

The first benchmark problem is a model problem with a *convex* boundary. This is an interesting problem for our own purposes because we are presently unable with **THG** to take "reentrant" neutrons into account. Therefore, benchmarking **THG** on such a problem with codes taking this phenomenon into account is more relevant. The problem consists in 7 concentric hexagons with parallel edges as depicted in Fig. 4.

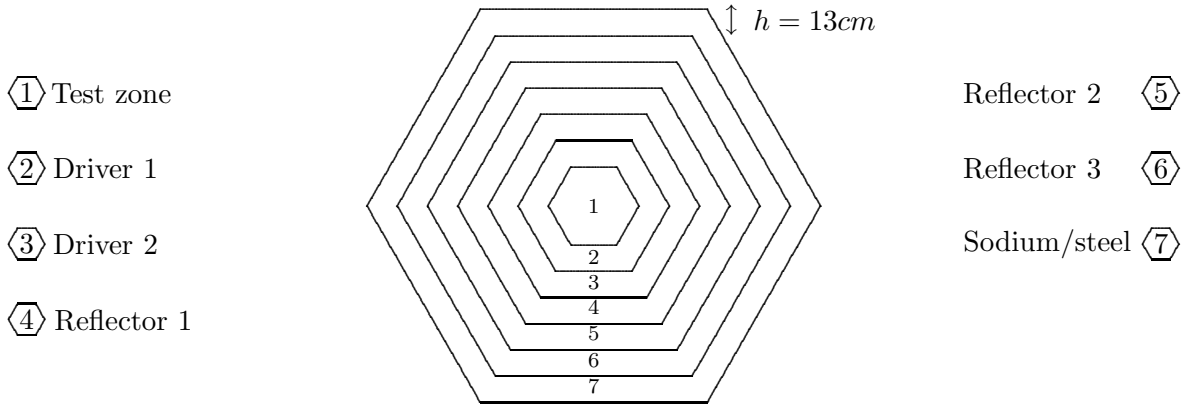

Figure 4: Simplified hexagonal core without reentrant external boundary

Table 2 displays k_{eff} calculations and discrete convergence orders (denoted α) obtained with DIAMANT2 and **THG** using the $RT0$ and $RT1$ nodal schemes. The benchmark solution to evaluate α is the $RT1$ calculation with a (2×2) mesh.

Table 2: k_{eff} values and convergence orders α for simplified fast breeder reactor with the DIAMANT2 code and the weakly discontinuous $RT0$ and $RT1$ nodal element schemes.

	DIAMANT2		$RT0$		$RT1$
Mesh	k_{eff}	α	k_{eff}	α	k_{eff}
1×1	1.491319	—	1.4912535	—	1.4920926
2×2	1.491860	1.73	1.4919734	2.80	1.4920945
4×4	1.492054	2.53	1.4920791	2.98	—
SPANDOM-$\triangle(h_1)$	1.49284		1.49284		1.49284
TWOHEX-$\triangle(h_1)/\triangle(h_2)$	1.49284/1.49208		1.49284/1.49208		1.49284/1.49208

One can see that the (4×4) $RT0$ and TWOHEX-$\triangle(h_2)$ calculation (with a triangle height equal to 1.625cm) give practically the same result. These results are much better than the SPANDOM-$\triangle(h_1)$ and TWOHEX-$\triangle(h_1)$ results where $h_1 = 6.5cm$. A higher value of α with the $RT0$ nodal element, makes the **THG** results closer to the benchmark value than the DIAMANT2 calculation with the same mesh. The $RT1$ results practically give the reference value.

The second benchmark problem is the modified 2D-SNR reactor configuration. The original problem is a four energy groups, two-dimensional fast reactor problem described in the ANL Benchmark Problem Book with the problem identification 18-A5 (see [13]). In the references [11,12] the authors modified the original problem by adding several radial blankets in the outer region of the core to obtain the hexagonal reactor configuration with $\pi/3$ symmetry shown on Fig. 5. For more details on this model problem, the readers should consult Refs [11,12].

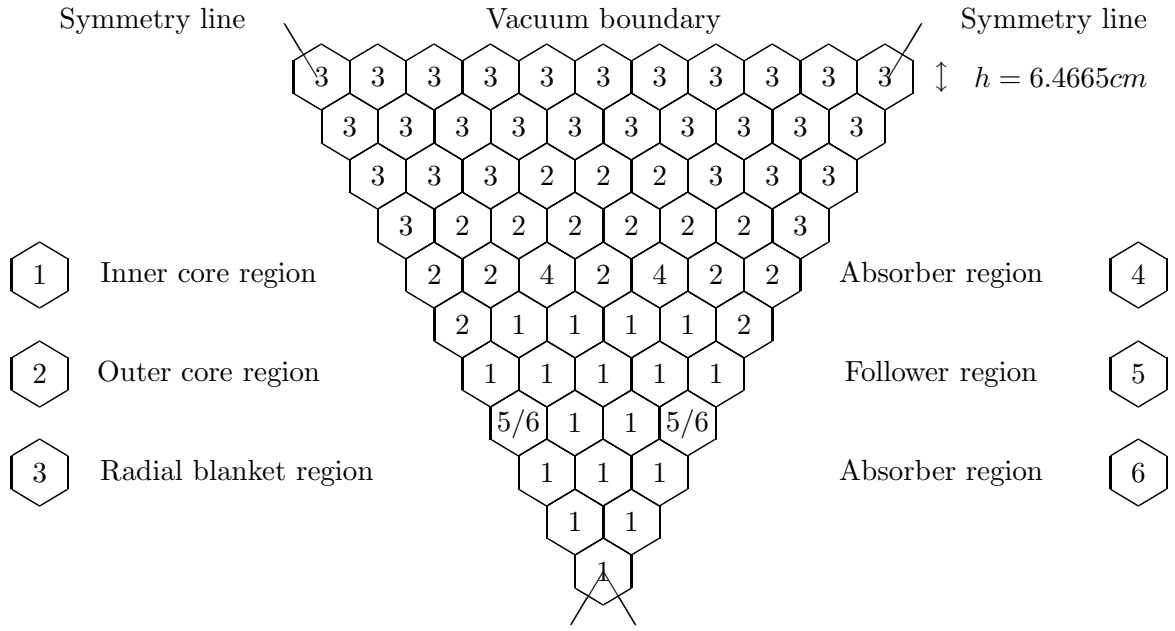

Figure 5: Modified 2D-SNR Benchmark problem, $\frac{\pi}{3}$ sector view

Table 3 gives the k_{eff} values obtained with DIAMANT2 and **THG** using the $RT0$ and $RT1$ schemes on two reactor configurations : control rods in (CRI) and out (CRO). Values obtained with SPANDOM, TWOHEX-6△, and TWOHEX-96△ borrowed from [11,12] are also indicated.

Table 3: k_{eff} values for the modified 2D-SNR benchmark problem, control rods in (CRI) and out (CRO) with the DIAMANT2 code and the weakly discontinuous $RT0$ and $RT1$ nodal element schemes.

	2D-SNR-CRI			2D-SNR-CRO		
	DIAMANT2	$RT0$	$RT1$	DIAMANT2	$RT0$	$RT1$
Mesh	k_{eff}	k_{eff}	k_{eff}	k_{eff}	k_{eff}	k_{eff}
1×1	1.13438	1.13433	1.13467	1.23697	1.23663	1.23683
2×2	1.13505	1.13483	1.13490	1.23716	1.23679	1.23682
4×4	1.13523	1.13492	—	1.23721	1.23686	—
SPANDOM	1.13901			1.23679		
TWOHEX-6△/96△	1.13784/1.13890			1.23616/1.23677		

Finally, the third benchmark problem is an hexagonal array where the central assembly is surrounded by 7 layers (a total amount of 169 assemblies) with 8 different compositions. For the

rods-out case, the k_{eff} reference value (obtained with a TWOHEX calculation using 96 triangles per hexagon and an S_4 angular approximation) is 1.30945 as shown on Table 4.

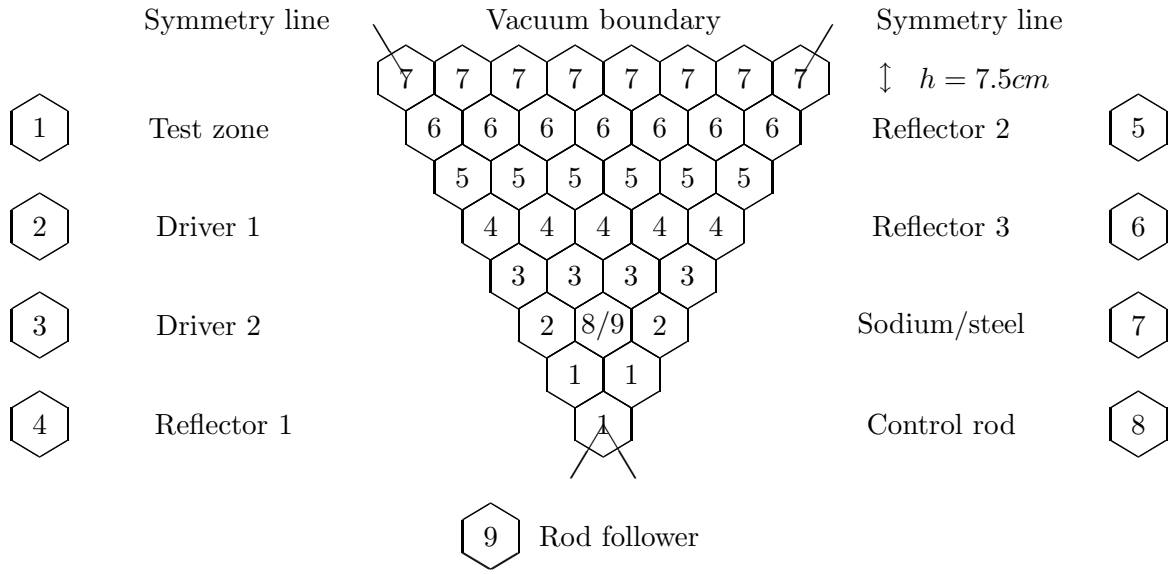

Figure 6: 2D-KNK Benchmark problem, $\frac{\pi}{3}$ sector view

Table 4: k_{eff} values for the 2D-KNK benchmark problem control rods in (CRI) and out (CRO) with the DIAMANT2 code and the weakly discontinuous $RT0$ and $RT1$ nodal element schemes.

	2D-KNK-CRI			2D-KNK-CRO		
	DIAMANT2	$RT0$	$RT1$	DIAMANT2	$RT0$	$RT1$
Mesh	k_{eff}	k_{eff}	k_{eff}	k_{eff}	k_{eff}	k_{eff}
1×1	1.00068	1.00611	1.00546	1.30714	1.30815	1.30880
2×2	1.00567	1.00053	1.00728	1.30841	1.30873	1.30887
4×4	1.00707	1.00744	1.00755	1.30878	1.30884	1.30886
SPANDOM	1.01055			1.30833		
TWOHEX-6△/96△	1.00454/1.00941			1.30833/1.30945		

The discrepancy with the SPANDOM and TWOHEX values is (partly) due to the fact that these codes take care of neutrons that, escaping from the outer boundary, may penetrate again into the reactor because of the nonconvex outer boundary. This effect doesn't occur with the first benchmark problem and our results are quite closer to the reference value given in [11,12]. It is worth mentioning that the (2×2) $RT1$ results for the last three benchmark problems involves approximately half the number of degrees of freedom of the reference TWOHEX calculation.

CONCLUSION

As a conclusion, we may state that the numerical efficiency of two-dimensional transport nodal finite element schemes may be readily applied to complex problems in hexagonal geometry, as shown in this paper. Work must be done however, to cope with reentrant neutrons in the

general nonconvex situation. A thorough analysis should be made also to "benchmark" reaction rates and angular fluxes. Finally, one should explore still higher RTk schemes in tricky reactor configurations where the $RT1$ nodal scheme might be less efficient.

ACKNOWLEDGEMENTS

The first author acknowledges the support of the Mexican Research Council (CONACyT) to the research project 33806-U as well as the financial support and hospitality at the Service de Métrologie Nucléaire (ULB) where this work was initiated during a 3 months sabbatical stay. The second author acknowledges continuous financial support from the Belgian FNRS.

REFERENCES

1. J.P. Hennart, "A General Family of Nodal Schemes", *SIAM J. Sci. Stat. Comput.*, **7**, 264–287, (1986).
2. J.P. Hennart and E. del Valle, "A Generalized Nodal Finite Element Formalism for Discrete Ordinates Equations in Slab Geometry. Part I: Theory in the Continuous Moment Case", *Transport Theory Statist. Phys.*, **24**, 449–478, (1995).
3. J.P. Hennart and E. del Valle, "A Generalized Nodal Finite Element Formalism for Discrete Ordinates Equations in Slab Geometry. Part II: Theory in the Discontinuous Moment Case", *Transport Theory Statist. Phys.*, **24**, 479–504, (1995).
4. B. Szabó and I. Babuška, *Finite Element Analysis*, John Wiley & Sons, New York, USA, (1991).
5. J.P. Hennart and E. del Valle, "On the Relationship between Nodal Schemes and Mixed-Hybrid Finite Elements", *Numer. Meth. for Partial Differ. Eqs.*, **9**, 411–430, (1993).
6. Y.Y. Azmy, "A Nodal Integral Method for Neutron Diffusion in Hexagonal Geometry", *Proceedings of the ANS Topical Meeting on Advances in Reactor Physics, Charleston, South Carolina*, **1**, 509, (1992).
7. J.P. Hennart, E.H. Mund and E. del Valle, "A Composite Nodal Finite Element for Hexagons", *Nucl. Sci. Eng.*, 127, 139–153, (1997).
8. J.P. Hennart and E. del Valle, "New Nodal Finite Element Schemes for the Discrete Ordinates Transport Equation", *Proceedings of the Joint International Conference on Mathematical Methods and Supercomputing for Nuclear Applications, Am. Nucl. Soc., Saratoga Springs*, **1**, 19–28, (1997).
9. K. Küfner, J. Burkhard and R. Heger, "An Updated FORTRAN-77 Version of the 2-D Static Neutron Transport Code DIAMANT2 for Regular Triangular Geometry", *Kernforschungszentrum Karlsruhe*, KfK-4133, (1987).
10. T. Takeda and H. Ikeda, "3-D Neutron Transport Benchmarks", *OECD/NEA Committee on reactor Physics (NEACRP)*, NEACRP-L-330 (1991).
11. T.H. Kim and N.Z. Cho, "Source Projection Analytical Nodal S_N Method for Hexagonal Geometry with Reentering Vacuum Boundary", *Trans. Am. Nucl. Soc.*, **75**, 171–174, (1996).
12. T.H. Kim and N.Z. Cho, "Source Projection Analytical Nodal S_N Method for Hexagonal Geometry", *Ann. Nucl. Energy*, **23**, 133–143, (1996).
13. ANL, "Benchmark Problem Book", ANL-7416, Suppl. 3, p. 861, (1985).